Rapid and simultaneous estimation of fault slip and heterogeneous lithospheric viscosity from postseismic deformation

T.T. Hines[1] and E.A. Hetland[1]

[1] *University of Michigan, Ann Arbor, MI, USA*

SUMMARY

Key words:

1 INTRODUCTION

Geodetic observations of surface deformation in the months to years following an earthquake are often attributed to afterslip (e.g. Marone et al. 1991), viscoelastic relaxation in the lithosphere (e.g. Nur & Mavko 1974), and/or poroelastic-relaxation (e.g. Peltzer et al. 1998; Jónsson et al. 2003). If postseismic deformation can be entirely described by afterslip, then one could easily constrain the spatial distribution of fault slip with a linear least squares inversion (e.g. Harris & Segall 1987; Bürgmann et al. 2002; Freed 2007), which could then provide insight into the frictional properties of faults (e.g. Hsu et al. 2006; Barbot et al. 2009). However, postseismic deformation following large (Mw≥7) earthquakes is often attributed to viscoelastic relaxation in the lithosphere (e.g. Hetland & Hager 2003; Pollitz 2003, 2005) or a combination of both afterslip and viscoelastic relaxation (e.g. Freed et al. 2006a; Hearn et al. 2008; Johnson et al. 2009; Rollins et al. 2015). In such cases, postseismic deformation can be used to constrain the viscous properties of the lithosphere, although this is a more difficult task than constraining a slip distribution. Not only are there potentially competing deformation mechanism which must be discerned, finding the viscosity distribution of the lithopshere from postseimsic deformation is a computationally expensive nonlinear inverse problem. Typically, this is approached with a forward modeling, grid search method. These forward modeling techniques require the number of unknown parameters being estimated to be small, meaning that significant and potentially inappropriate modeling assumptions must be made (Riva & Govers 2008; Hines & Hetland 2013).

    In this paper we propose a relatively fast method to kinematically invert coseismic and postseismic deformation to simultaneously estimate a time-dependent distribution of fault slip and an arbitrarily discretized viscosity structure of the lithosphere. Our method is based on an approximation which linearizes the rate of early postseismic deformation with respect to the viscosity of the lithosphere. We demonstrate the efficacy and limitations of our method through a synthetic test.

2 LINEARIZING EARLY POSTSEISMIC DEFORMATION

We assume that the lithosphere can be approximated as a Maxwell viscoelastic material on the timescales of postseismic deformation, where shear stress and strain are related by

$$\frac{\partial \boldsymbol{\varepsilon}}{\partial t} = \frac{\boldsymbol{\sigma}}{2\eta} + \frac{1}{2\mu}\frac{\partial \boldsymbol{\sigma}}{\partial t}. \tag{1}$$

η and μ are viscosity and shear modulus, respectively. This constitutive relationship implies that a sudden strain in the lithosphere from an earthquake will instantaneously propagate stresses through the lithosphere elastically (assuming the lithosphere is undergoing quasi-static deformation). Creep will also initiate immediately after the earthquake, where the initial viscous strain rate in each parcel of the lithosphere will be proportional to the fluidity ($\varphi = 1/\eta$) in that parcel, and independent of the fluidity elsewhere, as stress at this time is only controlled by the elastic properties. Each parcel will continue to creep at approximately that rate for as long as the initial elastic stresses from the earthquake are large compared to the stresses transferred throughout the lithosphere by viscoelastic relaxation. In this early postseismic period, creep in each parcel will express itself as surface deformation with an amplitude that is also proportional to the fluidity in that parcel and independent of the fluidity elsewhere. The early surface expression of creep in the entire lithosphere is therefore a sum of the surface expression of each parcel and is linear with respect to lithospheric fluidity. This property of early postseismic surface deformation is demonstrated below using simple infinite length, strike-slip earthquake models, where the lithosphere is approximated as a layered halfspace. The linearity of postseismic deformation with respect to fluidity to greatly facilitates the inverse problem of estimating lithospheric viscosity.

2.1   Two-dimensional earthquake models

The easiest way to demonstrate how postseismic deformation can be linearized with respect to lithospheric viscosity is with a simple two-dimensional earthquake model consisting of a long, vertical, surface rupturing, strike-slip fault that is embedded in a viscoelastic horizontal layer overlying a viscoelastic halfspace. We make use of the correspondence principle of viscoelasticity (e.g. Flügge 1975), which states that the Laplace transform of deformation in a viscoelastic body has the same form as the Laplace transform of deformation in a elastic body with the same geometry and subjected to the same boundary conditions. The solution for displacements following an earthquake in a viscoelastic lithosphere can then be easily found provided that the corresponding elastic solution is known (e.g. Nur & Mavko 1974; Savage & Prescott 1978; Hetland & Hager 2005). One only needs to replace the shear modulus in the Laplace transform of the elastic solution with the effective viscoelastic shear modulus and then compute the inverse Laplace transform.

2.1.1   Two layered model

From the solution of Rybicki (1971), surface displacements, $u_e(x, t)$, resulting from slip on a fault in an elastic surface layer overlying a semi-infinite elastic substrate are

$$u_e(x, t) = b(t) \left(\frac{1}{2} W(0) + \sum_{n=1}^{\infty} \Gamma^n W(n) \right), \tag{2}$$

where

$$W(n) = \frac{1}{\pi} \left(\tan^{-1} \left(\frac{2nH + D}{x} \right) - \tan^{-1} \left(\frac{2nH - D}{x} \right) \right) \tag{3}$$

and

$$\Gamma = \frac{\mu_1 - \mu_2}{\mu_1 + \mu_2}. \tag{4}$$

In the above equation, $b(t)$ describes cummulative slip on the fault through time and can describe coseismic slip and/or afterslip. D is the locking depth of the fault, H is the thickness of the upper layer, and μ_1 and μ_2 are the shear modulii in the upper layer and lower substrate, respectively. The Laplace transform of eq (2) is

$$\hat{u}_e(x, s) = \hat{b}(s) \left(\frac{1}{2} W(0) + \sum_{n=1}^{\infty} \Gamma^n W(n) \right). \tag{5}$$

We replace μ_1 and μ_2 in eq. 5 with the equivalent shear modulii for Maxwell materials in the Laplace domain, $\hat{\mu}_1$ and $\hat{\mu}_2$, to get the Laplace transform of surface displacements in the two-layered, viscoelastic half-space,

$$\hat{u}_v(x, s) = \hat{b}(s) \left(\frac{1}{2} W(0) + \sum_{n=1}^{\infty} \hat{\Gamma}^n W(n) \right), \tag{6}$$

where

$$\hat{\Gamma} = \frac{\hat{\mu}_1 - \hat{\mu}_2}{\hat{\mu}_1 + \hat{\mu}_2} \tag{7}$$

and

$$\hat{\mu}_i = \frac{s}{\frac{s}{\mu_i} + \frac{1}{\eta_i}}. \tag{8}$$

To find the surface displacements in the time domain one must find the inverse Lapace transform of eq (6), which is typically done using the method of residues. However, we are interested in characterizing the behavior of early postseismic deformation and it better serves us to instead perform the inverse Laplace transform with an extension of the initial value theorem (Appendix A). We assume for simplicity that the shear modulus for the viscoelastic lithosphere is homogenous (i.e. $\mu_1 = \mu_2$) and demonstrate in a supplementary IPython notebook that our conclusions still hold when $\mu_1 \neq \mu_2$. The surface displacements in the time domain are

$$u_v(x, t) = b(t) \frac{1}{2} W(0) + b(t) * \mathcal{L}^{-1} \left[\sum_{n=1}^{\infty} \hat{\Gamma}^n W(n) \right]. \tag{9}$$

Evaluating the above inverse Laplace transform using the method described in Appendix A, we find

$$\begin{aligned} u_v(x, t) = &b(t) \frac{1}{2} W(0) + \\ &b(t) * \left(\frac{\mu}{2\eta_2} W(1) - \frac{\mu}{2\eta_1} W(1) \right) + \\ &b(t) * \left(\left(\frac{\mu^2 t}{4\eta_2^2} - \frac{\mu^2 t}{4\eta_1 \eta_2} \right) (W(1) - W(2)) + \left(\frac{\mu^2 t}{4\eta_1 \eta_2} - \frac{\mu^2 t}{4\eta_1^2} \right) (W(1) + W(2)) \right) + \\ &\dots . \end{aligned} \tag{10}$$

Rapid and simultaneous estimation of fault slip and heterogeneous lithospheric viscosity from postseismic deformation

The first term in eq (10) is the elastic response to slip on the fault. The remaining terms describe the surface displacement due to viscoelastic relaxation. The first of these remaining terms is the initial viscoelastic response and, as suggested, it is a linear expression with respect to the fluidity in each of the two layers.

If the time since the rupture is sufficiently small compared to the relaxation times of each layer, $\tau_i = \eta_i/\mu$, (i.e. the third and following terms in eq. (10) are small), then we can truncate the series and approximate early surface deformation using only the elastic response and the initial viscoelastic response,

$$u_v(x,t) \approx b(t)\frac{1}{2}W(0) + \int_0^t b(\theta)\left(\frac{\mu}{2\eta_2}W(1) - \frac{\mu}{2\eta_1}W(1)\right)d\theta. \tag{11}$$

An approximation similar to eq. (11) was demonstrated by Segall (2010) for an elastic layer over a Maxwell viscoelastic substrate.

Figure 1 shows the series solution from eq. (10) truncated at a sufficiently large N along with the approximation given by eq. (11). In this comparison, we use $H = 15$ km, $D = 10$ km and a shear modulus of 32.0 GPa throughout the lithosphere. The upper layer is given a viscosity of 10^{20} Pa s ($\tau \approx 100$ years) and the substrate is given a viscosity of 10^{19} Pa s ($\tau = 10$ years). We let b(t) describe a unit of instantaneous slip at $t = 0.0$. We find the that the approximate solution is a good representation to the series solution for at least as long as half the lowest of the two relaxation time, regardless of our choice of model parameters. The approximation breaks down faster than what is show in Figure 1 when the upper layer is weaker than the substrate or when we decrease the depth of the material interface (i.e. when the weaker material is closer to the fault). We also note that the approximation has more longevity for locations further away from the fault, where it starts to break down at about $\min(\tau_i)$.

It is worth noting that the initial viscoelastic response for the uppermost layer and lower half-space differ only in sign and in amplitude. In the context of an inverse problem, this means that it is impossible to use (11) to estimate the absolute viscosity of the two layers, rather it is only possible to estimate their relative viscosities. This is not a difficult obstacle to overcome because in application we can typically assume that the upper layer has a sufficiently long Maxwell relaxation time such that it is effectively elastic over the postseismic period.

2.1.2 Three layered model

We follow the same procedure from above to find the surface deformation resulting from slip on a strike-slip fault in a three layered viscoelastic half-space. Starting from the layered elastic solution from Chinnery & Jovanovich (1972), we evalutate the solution for the viscoelastic problem in our supplementary ipython notebook. Once again, we find that the initial viscoelastic response to a unit of slip, given by

$$\frac{\partial}{\partial t}u_v(x,t) = \frac{\mu}{2\eta_3}W(1,1) + \frac{\mu}{2\eta_2}(W(0,1) - W(1,1)) - \frac{\mu}{2\eta_1}W(0,1), \tag{12}$$

where

$$W(n,m) = \frac{1}{\pi}\left(\tan^{-1}\left(\frac{2nH_2 + 2mH_1 + D}{x}\right) - \tan^{-1}\left(\frac{2nH_2 + 2mH_1 - D}{x}\right)\right), \tag{13}$$

is linear with respect to the fluidity in each of the three layers. We can approximate early postseismic deformation resulting from slip described by $b(t)$ in the same manner as in section 2.1.1 as

$$u_v(x,t) \approx b(t)\frac{1}{2}W(0,0) + \int_0^t b(\theta)\left(\frac{\mu}{2\eta_3}W(1,1) + \frac{\mu}{2\eta_2}(W(0,1) - W(1,1)) - \frac{\mu}{2\eta_1}W(0,1)\right)d\theta, \tag{14}$$

where η_1, η_2, and η_3 are the viscosities of the top, middle, and bottom layers, respectively, and H_1 and H_2 are the thicknesses of the top and middle layer, respectively. We can see that eq. (14) recovers eq. (11) when $\eta_3 = \eta_2$.

2.1.3 Continuous depth dependent model

At this point we posit that a similar approximation can be made for an arbitrarily layered lithosphere. In Appendix B we use eq. (11) to find an initial viscoelastic response kernel. We then integrate that kernel over the depth of the lithosphere to find the initial viscoelastic response for an arbitrary depth dependent viscosity structure. If the lithsophere is elastic above the fault depth, D, and described by $\eta(z)$ below D then early postseismic deformation can be approximated as

$$u(x,t) \approx \frac{b(t)}{\pi}\tan^{-1}(\frac{D}{x}) + \int_o^t \int_D^\infty \frac{\mu b(\theta)}{2\pi\eta(z)}\left(\frac{2x}{x^2 + (D+2z)^2} - \frac{2x}{x^2 + (2z-D)^2}\right)dzd\theta. \tag{15}$$

Although the above equation is capable of describing surface deformation for an arbitrary depth dependent viscosity structure, it falls short of being useful as the forward solution in an inverse problem aimed at estimating lithospheric viscosity. This shortcoming is because the above equation makes the unphysical assumption that the fault is infinitely long, in addition to the restriction of only being applicable to a vertical strike-slip fault. The assumption of infinite length would introduce first order errors, which would likely wash out the second order effect of viscosity. However, eq. (15) is useful for making estimates of the depth sensitivity of postseismic deformation.

2.2   arbitrarily discretized earthquake models

Motivated by our above results, we make the assertion that the initial rate of surface deformation resulting from an instantaneous dislocation in a three-dimensional Maxwell viscoelastic medium, which has been arbitrarily discretized into N regions, will have the form

$$\frac{\partial}{\partial t}\vec{u}(\vec{x},t)\big|_{t=0} = \sum_{j}^{N} \frac{1}{\eta_j} G_j(\vec{x}). \tag{16}$$

We denote $\vec{u}$ and $\vec{x}$ as vectors to emphasize that eq. (16) is generalized to three-dimensional problems. We use $G_j(\vec{x})$ to represent the initial rate of surface deformation at position $\vec{x}$ resulting from viscoelastic creep in region j with unit fluidity, where fluidity is zero (i.e. elastic) in all other regions. In this sense, $G_j(x)$ can be thought of as a Green's function for the initial rate of surface deformation resulting for viscoelastic deformation, and thus we refer to $G_j(x)$ as the initial viscoelastic Green's function. We verify eq. (16) numerically in section 5.5 and save a theoretical justification for a later paper.

Using eq. (16), we can then approximate early surface deformation as

$$\vec{u}(\vec{x},t) \approx b(t)F(\vec{x}) + \sum_{j}^{N} \int_{0}^{t} \frac{b(\theta)}{\eta_j} G_j(\vec{x})d\theta, \tag{17}$$

where $F(x)$ is the elastic Green's function, which describes the elastic deformation resulting from a dislocation. We further generalize the approximation of surface deformation in eq. (17) to allow for an arbitrary spatial distribution of slip by using linear superposition. If the elastic defomation in a viscoelastic lithosphere can be described in terms of M elastic dislocation sources, then early surface deformation resulting from both elastic dislocations and viscous creep can be approximated as

$$\vec{u}(\vec{x},t) \approx \sum_{i}^{M} b_i(t)F_i(\vec{x}) + \sum_{i}^{M}\sum_{j}^{N} \int_{0}^{t} \frac{b_i(\theta)}{\eta_j} G_{ij}(\vec{x})d\theta. \tag{18}$$

The initial viscoelastic Green's function is dependent upon both the region it represents as well as the dislocation source which induces the viscoelastic creep in that region, hence the two indices. It is worth restating that the approximation given above does not account for the viscoelastic coupling between the regions, since each region's contribution to surface deformation is independent of the viscosity elsewhere in eq.(18). This approximation is therfore appropriate for as long as the regions do not significantly transfer stresses between eachother through viscoelastic deformation.

3   INVERSION METHOD

The approximation of postseismic deformation given by eq. (18) can be cast as an inverse problem aimed at finding the distribution of slip on a fault and an arbitrarily complicated lithosphere viscosity structure from postseismic deformation. We assume that the slip history in any one direction on each fault patch, $b_i(t)$, can be expressed as P linear terms such that

$$b_i(t) = \sum_{k}^{P} \alpha_{ik} A_k(t), \tag{19}$$

where $A_k(t)$ consists of either step functions describing coseismic slip on a fault patch, or ramp functions, which have nonzero slope over a time interval and are intended to represent afterslip. α_{ik} then represents either the amount of coseismic slip of the cumulative slip over a time interval. The approximation given by eq. (18) now becomes

$$\vec{u}(\vec{x},t) \approx \sum_{i}^{M}\sum_{k}^{P} \alpha_{ik} F_i(\vec{x})A_k(t) + \sum_{i}^{M}\sum_{j}^{N}\sum_{k}^{P} \int_{0}^{t} \frac{\alpha_{ik}}{\eta_j} G_{ij}(\vec{x})A_k(\theta)d\theta. \tag{20}$$

If we assume a fault geometry and the elastic properties of the lithosphere, $F_i(\vec{x})$ can be computed with finite element software or with an analytical solution (e.g. Okada 1992; Meade 2007). Likewise, $G_{ij}(\vec{x})$ can be computed using finite element software. If the assumed geometry of the viscoelastic regions is sufficiently simple, $G_{ij}(\vec{x})$ may also be computed with semi-analytic techniques (e.g. Pollitz 1997; Fukahata & Matsu'ura 2006; Barbot & Fialko 2010).

We estimate the unknown slip parameters, α_{ik}, and unknown viscosities in each region of the lithosphere, η_j from observations of surface deformation in a least squares sense. Let $\boldsymbol{u_{obs}}$ be a vector of observed coseismic and postseismic surface displacements at various locations and points in time. Let $\boldsymbol{m}$ be a vector of all the unknown parameters α_{ik} and η_j with length $Q = M + N + P$, and let $\boldsymbol{u}(\boldsymbol{m})$ be a vector of postseismic surface displacements predicted by eq (20). We seek to solve

$$\min \big|\big| \boldsymbol{f}(\boldsymbol{m}) \big|\big|_2^2 \tag{21}$$

subject to the constraint that

$$\boldsymbol{m} \geq 0, \tag{22}$$

where

$$\boldsymbol{f(m)} = \begin{vmatrix} \boldsymbol{W}\left(\boldsymbol{u(m)} - \boldsymbol{u}_{\mathrm{obs}}\right) \\ \lambda_s \boldsymbol{L_s m} \\ \lambda_v \boldsymbol{L_v m} \end{vmatrix}. \tag{23}$$

In the above equation, $\boldsymbol{W}$ is a diagonal matrix containing the reciprocal of the data uncertainties (i.e. $\boldsymbol{W^T W} = \boldsymbol{C_d}^{-1}$ where $\boldsymbol{C_d}$ is the data covariance matrix), and $\boldsymbol{L_s}$ and $\boldsymbol{L_v}$ are regularization matrices.

We impose a nonnegativity constraint on $\boldsymbol{m}$ which ensures that inferred slip is in one predominant direction and that viscosities are positive. Specifically, the rake of the inferred slip on each fault patch is to be within a $90°$ window defined by the rakes of chosen orthogonal basis slip directions. For instance, the basis slip directions could be chosen such that only slip rakes within $45°$ of pure strike-slip, normal, or thrust are permissible.

Because this inverse problem inevitably has nonunique solutions for $\boldsymbol{m}$, we put additional constraints on the inferred slip and inferred viscosity with the matrices $\boldsymbol{L_s}$ and $\boldsymbol{L_v}$, respectively. In our following synthetic tests, we constrain the solution by minimizing the Laplacian of the spatial distribution of fault slip and lithospheric viscosity. We do so by letting $\boldsymbol{L_s}$ and $\boldsymbol{L_v}$ be umbrella operators (Desbrun et al. 1999) such that they can be stacked on top of eachother into the matrix L_{ij}, which satisfies

$$\sum_j^Q L_{ij} m_j = \frac{1}{|\mathcal{N}(i)|} \sum_{k \in \mathcal{N}(i)} m_k - m_i. \tag{24}$$

In the above equation $\mathcal{N}(i)$ denotes the set of indices for model parameters describing slip (viscosity) which is adjacent to the slip (viscosity) described by m_i and $|\mathcal{N}(i)|$ is the length of that set.

The parameters λ_v and λ_s in eq. (23) control how much we enforce the smoothness constraint. We choose these parameters using L-curves, which describe the trade off between the model smoothness and data misfit (figure 6). We first set $\lambda_v = 0$ and then use an L-curve to pick $\lambda_s = 0$, then we fix λ_s at our chosen value and use another L-curve to pick λ_v. We have attempted to choose our model parameters through cross-validation but we found that the optimal pair of penalty parameters picked through cross-validation tended to significantly degrade our fit to the most near-field stations.

We find $\boldsymbol{m}$ that satisfies the above conditions using the Gauss-Newton method (e.g. Aster et al. 2013). The best fit model parameters are found by making an initial guess for the solution and then iteratively solving

$$\boldsymbol{J(m^k)m^{k+1}} = -\boldsymbol{f(m^k)} + \boldsymbol{J(m^k)m^k} \tag{25}$$

for $\boldsymbol{m^{k+1}}$. $\boldsymbol{J(m^k)}$ is the Jacobian of $\boldsymbol{f(m)}$ with respect to $\boldsymbol{m}$ evaluated at $\boldsymbol{m^k}$. We impose the nonnegativity constraint on $\boldsymbol{m}$ by solving eq. (25) with a nonnegative least squares algoritm (Lawson & Hanson 1995). We find that it is occasionally necessary to constrain the step size for each iteration of eq. (25) in order to ensure convergence. We do so in a manner akin to the Levenberg-Marquardt algorithm (e.g. Aster et al. 2013). We instead solve

$$\boldsymbol{J^*(m^k)m^{k+1}} = -\boldsymbol{f^*(m^k)} + \boldsymbol{J^*(m^k)m^k} \tag{26}$$

for m^{k+1}, where

$$\boldsymbol{J^*(m)} = \begin{vmatrix} \boldsymbol{J(m)} \\ \kappa \boldsymbol{I} \end{vmatrix}, \tag{27}$$

and

$$\boldsymbol{f^*(m)} = \begin{vmatrix} \boldsymbol{f(m)} \\ \boldsymbol{0} \end{vmatrix}, \tag{28}$$

and κ controls the step size for each iteration and varies depending on whether the algorithm is converging.

In a nonlinear least squares algorithm, computing the Jacobian typically is the largest computational burden; however, in this case evaluating the Jacobian of eq. (20) requires only a few computationally inexpensive matrix operations. Consequently, our nonlinear least squares algorithm converges to a solution for $\boldsymbol{m}$ in a matter of seconds on a desktop computer. The main computational burden is in computing $F_i(x)$ and $G_{ij}(x)$ which is done with finite element software and only needs to be done once for a given fault and lithosphere geometry. Throughout this paper, our initial guess for the model parameters is that there is no slip on any fault patch, and the lithosphere is entirely elastic ($1/\eta = 0$). In our experience, the choice of initial guess has an insignificant effect on the best fit solution.

4 SYNTHETIC TEST

4.1 Synthetic postseismic deformation

We demonstrate with a synthetic test that our inverse method is capable of recovering fault slip and lithospheric viscosity from postseismic deformation. We use the finite element software, Pylith (Aagard et al. 2013), to compute the surface deformation resulting from a specified amount of slip on a fault in a lithosphere with a specified viscosity. We invert this synthetic surface deformation using the method described above to recover the imposed model parameters. The synthetic test also serves to demonstrate that eqs. (16) and (18) are indeed valid for three dimensional earthquake models.

Our synthetic model consists of a 50 km long by 20 km wide strike-slip fault, striking to the north and dipping $60°$ to the east (figure

4). At $t = 0.0$ we impose $6.54 * 10^{19}$ N m of surface rupturing, right-lateral coseismic slip with a distribution shown in Figure 2. After the coseismic slip, we impose a constant rate of afterslip from $t = 0.0$ to $t = 0.5$ years. The cumulative seismic moment over this interval is about $1.07 * 10^{19}$ N m. The spatial distribution of afterslip is shown in Figure 2. During the interval $t = 0.5$ to $t = 1.0$, years the rate of afterslip is decreased by a factor of 2. From $t = 1.0$ year onward, we do not impose any fault slip.

The lithosphere in our synthetic model is Maxwell viscoelastic with homogenous Lamé parameters $\lambda = 32.0$ GPa and $\mu = 32.0$ GPa. The viscosity in the lithosphere decays from 10^{21} Pa s ($\tau \approx 1,000$ years) at the surface to 10^{19} Pa s ($\tau \approx 10$ years) at 75 km depth (Figure 3). We compute displacements at 0.1 year intervals up until $t = 10$ years, which makes the upper layer effectively elastic on these timescales. We compute surface displacements at 60 randomly chosen locations within a 400 km square centered about the fault (Figure 4). This is intended to roughly correspond with the density of GPS station at a well instrumented plate boundary. We add temporally correlated noise to the computed displacements through time consistent with what one would expect from GPS observations. The standard deviation of northing and easting displacements is 1.0 mm, and the standard deviation of the vertical displacements is 2.5 mm. We add temporal covariance with an exponential noise model that has a characteristic timescale of 0.25 years, which is intended to simulate seasonal processes that are typically present in GPS time series.

4.2   Green's functions

We invert the synthetic surface deformation for fault slip on a 4 km by 4 km discretization of the fault segment and we estimate a constant viscosity in 10 km thick horizontal layers from the surface down to 70 km depth. We compute the elastic Green's functions, $F_i(\vec{x})$, and initial viscoelastic Green's functions, $G_{ij}(\vec{x})$, numerically using Pylith. The elastic Greens functions are the initial surface displacements resulting from 1.0 m of imposed slip on fault patch i. For each fault patch, we use basis slip directions with rake $45°$ updip and $45°$ downdip of pure right-lateral slip. These slip basis directions restrict all inferred slip to be within $45°$ of right-lateral. We find the initial viscoelastic Green's functions, $G_{ij}(\vec{x})$, by computing the initial rate of surface deformation due to 1.0 m of slip on fault patch i in a model that is elastic everywhere except in region j, which is assigned a viscosity of 10^{18} Pa s.

We define the basis slip functions, $A_k(t)$, as a heaviside function centered at $t = 0.0$ and three ramp functions which increase from 0.0 to 1.0 m of slip over the time intervals $0.0 \leq t < 0.5$ years, $0.5 \leq t < 1.0$ years, and $1.0 \leq t < 10.0$ years. Although our synthetic model does not have any fault slip during the last time interval, we include it to test if postseismic deformation over that interval, which is resulting purely from viscoelastic creep in the synthetic model, can be describe with continued fault slip.

4.3   Recovered model

Our best fitting model of slip on the fault is shown in Figure 2. The spatial distribution and direction of inferred the coseismic slip are a good match to the synthetic coseismic slip. The distribution of afterslip was decently recovered but not as well as for the coseismic slip. There are a few artifacts in the distribution of afterlsip which are not present in the synthetic model, such as slip on the north-most and deepest section of the fault. We attribute these artifacts to data noise. The distribution of afterslip is more diffuse than in the synthetic model, which is a result of our regularization scheme. The inability to recover the details of the imposed afterslip could be because the data noise is obscuring some of the postseismic signal or possibly because the imposed afterslip is deeper than the coseismic slip and thus more difficult to accurately recover. Nevertheless, the inferred moment of both coseismic slip and afterslip, which is proportional to slip integrated over the fault plane, is in good agreement with the moment in the synthetic model. Although the spatial distribution of inferred slip may be more difficult to recover, the cumulative slip seems to be consistently recovered with ease.

The inferred slip over the last time interval, 1.0 to 10.0 years following the earthquake, is also consistent with the synthetic model. The seismic moment of slip over this interval is $5 * 10^{17}$ N m, which is two orders of magnitude smaller than the moment for the coseismic slip. This means that the inferred slip is accounting for, at most, a few mm's of displacement from $t = 1.0$ to $t = 10.0$ years. This is on order of the data uncertainty and so the inferred slip is negligably small. The surface deformation during this time interval is therefor being properly attributed to viscoelastic relaxation.

The inferred viscosities in each of the eight layers are shown in figure 3a. The recovered viscosities correspond well with the synthetic model except perhaps for the top layer from 0 to 10 km depth. We used bootstrapping to estimate the uncertainties of the recovered viscosities and we found that the strongest layers near the surface, despite being proximal to the earthquake source, have the highest uncertainties. However, viscosities greater than 10^{20} Pa s are effectively elastic on the timescales of this synthetic test and so a wide range of high viscosities for the upper layers would just as adequately be able to describe the synthetic surface displacements. When looking at inferred values of fluidity (figure 3b), we see that the uncertainties are lowest at the surface and increase with depth, as is perhaps more intuitive.

4.3.1   Validation

The fact that our recovered fault slip and lithospheric viscosity are in good agreement with the synthetic model suggests that the approximation given by eq. (18) is accurate over the ten years of synthetic data. We quantify the accuracy of eq. (18) by running a forward model with Pylith where the imposed fault slip and lithospheric viscosity are those found in our recovered model. We then compare the displacements from the numerically computed forward model with the displacements predicted by eq. (18). We refer to the numerically computed displacements as $\boldsymbol{u}_{\text{true}}(t)$ and the displacments predicted by our approximation as $\boldsymbol{u}(t)$. We define the approximation residuals as $\boldsymbol{u}(t) - \boldsymbol{u}_{\text{true}}(t)$.

At $t = 10.0$ years the approximation residuals are on order of a couple mm's in length for each location and are small compared to the cm's of deformation resulting from viscoelastic relaxation (figure 7), indicating that eq. (18) is indeed a fair approximation. At $t = 20$ years the approximation residuals are about one cm in magnitude for near field sites, while the residuals are still on order of a few mm's for

the far field sites. The faster divergence for the near field sites is consistent with the comparison we made between the approximate and true displacements for a two-dimensional, two layered earthquake model in section 3.1.1.

we include circles with radius 1 mm centered at each station to illiustrate how large the error is with respect to the data noise

The accuracy of eq. (18) is also demonstrated in figure 5, which shows $\boldsymbol{u}(t)$ and $\boldsymbol{u}(t)_{\text{true}}$ at a sample site near the fault. The numerical solution asymptotically approaches the rate of deformation predicted by eq. (18) as time goes to zero, demonstrating that eq. (16) accurately descibes the initial viscoelastic response. Additionally, the magnitude of the difference between $\boldsymbol{u}(t)$ and $\boldsymbol{u}_{\text{true}}(t)$ is smaller than the uncertainty on our synthetic data throughout the time series, indicating that our approximation is appropriate for this synthetic test.

Note the duration of the approximation and how it is longer than in 3d

5 DISCUSSION

A fundemental assumption in our method for estimating slip and viscosity from postseismic deformation is that the timescale of relaxation in the lithosphere is at least as long as the timescales over which postseismic deformation is observed. This assumption allows us to approximate the surface expression of viscous creep as a linear system with respect to lithospheric fluidity, which greatly facilitates and expedites the inverse problem. However, the lithosphere's relaxation time is generally not well known. There is then an added complication of deciding how much of the postseismic time series to use in the inverse problem. In our synthetic example, we conveniently picked the length of our time series to correspond with the weakest relaxation time in the lithosphere; however, the length of the time series could have also been determined iteratively. For example, if the approximation given by eq. (18) is incapable of adequately describing the observed postseismic deformation, then it is possible that the length of the time series used in the inversion exceeds the time interval over which eq. (18) is appropriate. One can reduce the length of the postseismic time series used in the inversion until an adequate fit is found.

postseismic deformation following large ($\geq Mw = 7$) earthquakes often is characterized by rapid early transience which decays to a steady rate after a matter of months (e.g. Savage & Svarc 1997; Savage et al. 2005; Ergintav et al. 2009; Rollins et al. 2015). This pattern (better word?) of surface deformation is difficult to recreate soley with creep in a Maxwell viscoelastic lithosphere. Several studies have explored other lithospheric rheologies to explain observed transient postseismic deformation. For example, Pollitz (2003, 2005) invoked a Burgers rheology upper mantle to explain surface displacements following the 2002 $Mw = 7.9$ Denali earthquake and the 1999 $Mw7.1$ Hector Mine earthquake. In both cases the best fitting transient relaxation time was on the order of a month and the best fitting steady state relaxation time was on the order of years. Postseismic deformation following the Denali earthquake was also successfully modeled by Freed et al. (2006b) with a power-law rheology in the upper mantle, consistent with laboratory studies (e.g. Kirby and Kronenberg 1987). The power-law rheology was able to reproduce the observed transient surface deformation because the high stresses in the earthquake decreased the effective viscosity of the upper mantle to 10^{17} Pa s resulting in fast surface deformation. As stresses from the earthquake relaxed, the effective viscosity increased and the predicted surface deformation became steadier.

Based on the success of Pollitz (2003, 2005) and Freed et al. (2006b), one may dismiss our method as being unrealistic because we assume that the lithosphere is Maxwell viscoelastic. However, our method does not necessarily preclude the possibility of a Burgers rheology or a stress-nonlinear viscosity. As long as stresses in the lithosphere remain roughly equal to the the stresses transferred elastically through fault slip then a viscosity structure inferred using our method could be interpretted as the effective viscosity for either a Burgers rheology of a power-law rheology. If the commonly observed early transient postseismic deformation truly is the result viscous relaxation in the lithosphere, then the results from Pollitz (2003, 2005) and Freed et al. (2006a) suggest that the time interval over which eq. (18) is appropriate is on order of a month after an earthquake. Although one month of postseismic data is a short window, such a low effective viscosity in the upper mantle would yield a strong signal over this time. We postulate that the method described in this paper would then be able to identify the location of the weak regions in the lithosphere with much higher resolution than what could be obtained through the typical forward modeling grid search method. Any excised portion of the timeseries could then be used to further constrain estimates of fault slip and lithospheric viscosity by including it in a gradient based nonlinear inverse method where the forward problem is computed numerically rather that with eq. (18). In such case, the initial guess for the model parameters would be the estimate of slip and viscosity made using the truncated time series.

The characteristic temporal evolution of postseismic deformation has also been described with a combination afterslip and relaxation in a Maxwell viscoelastic lithosphere (e.g. Perfettini et al. 2005; Johnson et al. 2009). In such models, the rapid early transient deformation is controlled by fault slip, while the later steady postseismic deformation is controlled by viscous relaxation in a relatively strong lithosphere (relaxation time of years the decades). Indeed, our synthetic data is characterized by transient near field surface deformation, caused by fault slip, followed by a steady rate of more diffuse surface deformation, resulting from viscous creep (figures 4 and 5). In such case our method could be applicable over a postseismic time series extending from the time of the earthquake out to years or decades.

6 CONCLUSION

APPENDIX A: INVERSE LAPLACE TRANSORM THROUGH SERIES EXPANSION

let $f(t)$ be analytic at $t = 0$ and let there be a real valued M, and C such that

$$\left| f^{(n)}(t) \right| < Ce^{Mt} \quad \forall t \geq 0 \text{ and } \forall n \in \{0, 1, 2, \dots\}, \tag{A.1}$$

where $f^{(n)}(t)$ denotes the nth derivative of $f(t)$. We define the Laplace transform of $f(t)$ as

$$\mathcal{L}[f(t)] := \hat{f}(s) := \int_0^\infty f(t)e^{-st}dt \tag{A.2}$$

and we restrict our attention to $s \in \mathbb{R}$. The constraints on $f^{(n)}(t)$ from eq. (A.1) ensure that

$$\lim_{s \to \infty} \mathcal{L}[f^{(n)}(t)] = 0. \tag{A.3}$$

It can be shown using integration by parts that

$$\mathcal{L}[f^{(n)}(t)] = s^n \hat{f}(s) - \sum_{m=1}^{n} s^{m-1} f^{(n-m)}(0) \quad \forall s > M. \tag{A.4}$$

Substituting eq. (A.4) into eq. (A.3) and then rearranging the terms gives us a recursive formula for $f^{(n)}(0)$ in terms of $\hat{f}(s)$:

$$f^{(n)}(0) = \lim_{s \to \infty} s^{n+1} \hat{f}(s) - \sum_{m=1}^{n} s^m f^{(n-m)}(0), \tag{A.5}$$

where the base case, $n = 0$, is the initial value theorem:

$$f(0) = \lim_{s \to \infty} s \hat{f}(s). \tag{A.6}$$

Since we request $f(t)$ to be analytic at $t = 0$, we can construct a Taylor series expansion of $f(t)$ such that

$$f(t) = \sum_{n=0}^{\infty} \frac{f^{(n)}(0)}{n!} t^n \quad \forall t \in D, \tag{A.7}$$

where D is some neighborhood of $t = 0$. We find the inverse Laplace transform of $\hat{f}(s)$ for $t \in D$ by combining eq. (A.7) with eqs. (A.5) and (A.6) so that $f(t)$ is expressed in terms of $\hat{f}(s)$.

APPENDIX B: POSTSEISMIC APPROXIMATION FOR A TWO-DIMENSIONAL EARTHQUAKE MODEL WITH AN ARBITRARY DEPTH DEPENDENT VISCOSITY

We seek to find an approximation for early postseismic deformation in a two-dimensional, strike-slip earthquake model with an arbitrary depth-dependent viscosity below the fault locking depth, D. We first find the initial rate of surface deformation following a unit of slip in a lithosphere that is elastic except for a viscoelastic layer which is at depth z and with thickness Δz. This is found by making the substitions $H_1 \to z$, $H_2 \to \Delta z$, $\eta_1 \to \infty$, $\eta_3 \to \infty$, and $\eta_2 \to \eta$ in eq. (12), which gives us

$$\frac{\partial}{\partial t} u_1(x,t)\big|_{t=0} = \frac{1}{\eta}(W(z + \Delta z) - W(z)), \tag{B.1}$$

where

$$W(z) = \frac{\mu}{2\pi} \left(\tan^{-1}\left(\frac{2z - D}{x}\right) - \tan^{-1}\left(\frac{2z + D}{x}\right) \right). \tag{B.2}$$

From eq. (16) we know that the initial rate of surface deformation for a lithosphere composed of N discrete layers, each with viscosity η_i, at depth z_i, and having thickness Δz, is then

$$\frac{\partial}{\partial t} u_N(x,t)\big|_{t=0} = \sum_{i}^{N} \frac{1}{\eta_i}(W(z_i + \Delta z) - W(z_i)). \tag{B.3}$$

The initial rate of surface deformation for a viscosity structure given by $\eta(z)$ is found by taking the limit as $\Delta z \to 0$ and $N \to \infty$:

$$\frac{\partial}{\partial t} u(x,t)\big|_{t=0} = \int_{D}^{\infty} \frac{1}{\eta(z)} \frac{\partial}{\partial z} W(z) dz \tag{B.4}$$

$$= \int_{D}^{\infty} \frac{\mu}{2\pi\eta(z)} \left(\frac{2x}{x^2 + (D + 2z)^2} - \frac{2x}{x^2 + (2z - D)^2} \right) dz. \tag{B.5}$$

Finally, we add the elastic component of deformation and integrate eq. (B.5) with the fault slip history to obtain an approximation for early postseismic deformation:

$$u(x,t) \approx \frac{b(t)}{\pi} \tan^{-1}(\frac{D}{x}) + \int_{o}^{t} \int_{D}^{\infty} \frac{\mu b(\theta)}{2\pi\eta(z)} \left(\frac{2x}{x^2 + (D + 2z)^2} - \frac{2x}{x^2 + (2z - D)^2} \right) dz d\theta. \tag{B.6}$$

REFERENCES

Aagaard, B.T., Knepley, M.G. & Williams, C.A., 2013. A domain decomposition approach to implementing fault slip in finite-element models of quasi-static and dynamic crustal deformation, *J. Geophys. Res. Solid Earth*, 118, doi: 10.1002/jgrb.50217.

Aster, R.C., Borchers, B., Thurber, C.H., 2013. Parameter estimation and inverse problems, *Academic Press*.

Barbot, S., Fialko, Y. & Bock, Y., 2009. Postseismic deformation due to the Mw 6.0 2004 Parkfield earthquake: Stress-driven creep on a fault with spatially variable rate-and-state friction parameters, *J. Geophys. Res. Solid Earth*, 114, 1-26. doi:10.1029/2008JB005748.

Rapid and simultaneous estimation of fault slip and heterogeneous lithospheric viscosity from postseismic deformation

Barbot, S. & Fialko, Y., 2010. A unified continuum representation of post-seismic relaxation mechanisms: Semi-analytic models of afterslip, poroelastic rebound and viscoelastic flow, *Geophys. J. Int.*, 182, 1124-1140. doi:10.1111/j.1365-246X.2010.04678.x.

Bürgmann, R., Ergintav, S., Segall, P., Hearn, E.H., McClusky, S., Reilinger, R.E., Woith, H. & Zschau, J., 2002. Time-dependent distributed afterslip on and deep below the İzmit earthquake rupture, *Bull. Seismol. Soc. Am.*, 92, 126-137. doi:10.1785/0120000833.

Chinnery, M.A. & Jovanovich, D.B., 1972. Effect of earth layering on earthquake displacement fields, *Bull. Seismol. Soc. Am.*, 62, 1629-1639.

Desbrun, M., Meyer, M., Schröder, P. & Barr, A.H., 1999. Implicit fairing of irregular meshes using diffusion and curvature flow, *Proceedings of the 26th Annual Conference on Computer Graphics and Interactive Techniques*, 317324. doi:10.1145/311535.311576.

Ergintav, S., McClusky, S., Hearn, E., Reilinger, R., Cakmak, R., Herrring, T., Ozener, H., Lenk, O. & Tari, E., 2009. Seven years of postseismic deformation following the 1999, M = 7.4 and M = 7.2, İzmit-Düzce, Turkey earthquake sequence. *J. Geophys. Res. Solid Earth*, 114. doi:10.1029/2008JB006021.

Flügge, W., 1975. Viscoelasticity, Springer-Verlag Berlin Heidelberg.

Freed, A.M., Bürgmann, R., Calais, E., Freymueller, J. & Hreinsdóttir, S., 2006. Implications of deformation following the 2002 Denali, Alaska, earthquake for postseismic relaxation processes and lithospheric rheology. *J. Geophys. Res. Solid Earth*, 111, 1-23. doi:10.1029/2005JB003894.

Freed, A.M., Bürgmann, R., Calais, E. & Freymueller, J., 2006. Stress-dependent power-law flow in the upper mantle following the 2002 Denali, Alaska, earthquake, *Earth Planet. Sci. Lett.*, 252, 481-489. doi:10.1016/j.epsl.2006.10.011.

Freed, A.M., 2007. Afterslip (and only afterslip) following the 2004 Parkfield, California, earthquake, *Geophys. Res. Lett.*, 34, 1-5. doi:10.1029/2006GL029155.

Fukahata, Y., Matsuura, M., 2006. Quasi-static internal deformation due to a dislocation source in a multilayered elastic/viscoelastic half-space and an equivalence theorem. *Geophys. J. Int.*, 166, 418-434. doi:10.1111/j.1365-246X.2006.02921.x.

Harris, R.A. & Segall, P., 1987. Detection of a locked zone at depth on the Parkfield, California, segment of the San Andreas Fault. *J. Geophys. Res.*, 92, 7945-7962. doi:10.1029/JB092iB08p07945.

Hirth, G. & Kohlstedt, D.L., 2003. Rheology of the Upper Mantle and the Mantle Wedge : A View from the Experimentalists, *Geophysical Monograph*, 138, 83-105. doi:10.1029/138GM06.

Hearn, E.H., McClusky, S., Ergintav, S. & Reilinger, R.E., 2009. İzmit earthquake postseismic deformation and dynamics of the North Anatolian Fault Zone. *J.Geophys. Res. Solid Earth*, 114, 1-21. doi:10.1029/2008JB006026.

Hetland, E.A. & Hager, B.H., 2005. Postseismic and interseismic displacements near a strike-slip fault: A two-dimensional theory for general linear viscoelastic rheologies. *J. Geophys. Res. Solid Earth*, 110, 1-21. doi:10.1029/2005JB003689.

Hetland, E.A. & Hager B.H., 2003. Postseismic relaxation across the Central Nevada Seismic Belt, *J. Geophys. Res.*, 108, 113. doi:10.1029/2002JB002257.

Hines, T.T. & Hetland, E.A., 2013. Bias in estimates of lithosphere viscosity from interseismic deformation, *Geophys. Res. Lett.*, 40, 4260-4265. doi:10.1002/grl.50839.

Hsu, Y.-J., Simons, M., Avouac, J.-P., Galetzka, J., Sieh, K., Chlieh, M., Natawidjaja, D., Prawirodirdjo, L. & Bock, Y., 2006. Frictional Afterslip Following the 2005 Nias-Simeulue Earthquake, Sumatra, *Science*, 312, 1921-1926.

Johnson, K.M., Bürgmann, R. & Freymueller, J.T., 2009. Coupled afterslip and viscoelastic flow following the 2002 Denali Fault, Alaska earthquake. *Geophys. J. Int.*, 176, 670-682. doi:10.1111/j.1365-246X.2008.04029.x.

Jónsson, S., Segall, P., Pedersen, R. & Bjornsson, G., 2003. Post-earthquake ground movements correlated to pore-pressure transients, *Nature*, 424, 179-183. doi:10.1038/nature01758.1.

Kirby, S.H. & Kronenberg, A.K., 1987. Rheology of the Lithosphere: Selected Topics. *Rev. Geophys.*, 25, 1219-1244.

Lawson, C.L. & Hanson, R.J., 1995. Solving least Squares Problems, SIAM.

Marone, C.J., Scholz, C.H. & Bilham, R., 1991. On the mechanics of earthquake afterslip, *J. Geophys. Res.*, 96, 8441-8452.

Meade, B.J., 2007. Algorithms for the calculation of exact displacements, strains, and stresses for triangular dislocation elements in a uniform elastic half space, *Computers and Geosciences*, 33, 1064-1075. doi:10.1016/j.cageo.2006.12.003.

Nur, A. & Mavko, G., 1974. Postseismic Viscoelastic Rebound, *Science*, 183, 204-206. doi:10.1126/science.183.4121.204.

Okada, Y., 1992. Internal deformation due to shear and tensile faults in a half space, *Bull. Seismol. Soc. Am.*, 82, 1018-1040.

Peltzer, G., Rosen, P., Rogez, F. & Hudnut, K., 1998. Poroelastic rebound along the Landers 1992 earthquake surface rupture. *J. Geophys. Res.*, 103, 30131-30145. doi:10.1029/98JB02302.

Perfettini, H., Avouac, J.P. & Ruegg J.C., 2005, Geodetic displacements and aftershocks following the 2001 Mw = 8.4 Peru earthquake: Implications for the mechanics of the earthquake cycle along subduction zones, *J. Geophys. Res. Solid Earth*, 110, 1-19. doi:10.1029/2004JB003522.

Pollitz, F.F., 1997. Gravitational viscoelastic postseismic relaxation on a layered spherical Earth. *J. Geophys. Res.*, 102, 17921-17941. doi:10.1029/97JB01277.

Pollitz, F.F., 2003. Transient rheology of the uppermost mantle beneath the Mojave Desert, California, *Earth Planet Sci. Lett.*, 215, 89-104. doi:10.1016/S0012-821X(03)00432-1.

Pollitz, F.F., 2005. Transient rheology of the upper mantle beneath central Alaska inferred from the crustal velocity field following the 2002 Denali earthquake, *J. of Geophys. Res. Solid Earth*, 110, 116. doi:10.1029/2005JB003672.

Riva, R.E.M. & Govers, R., 2009. Relating viscosities from postseismic relaxation to a realistic viscosity structure for the lithosphere. *Geophys. J. Int.*, 176, 614-624. doi:10.1111/j.1365-246X.2008.04004.x.

Rollins, C., Barbot, S. & Avouac, J-P. 2015, Postseismic Deformation Following the 2010 Mw7.2 El Mayor-Cucapah Earthquake: Observations, Kinematic Inversions, and Dynamic Models, *Pure Appl. Geophys.*, doi:10.1007/s00024-014-1005-6.

Rybicki, K., 1971. The elastic residual field of a very long strike-slip fault in the presence of a discontinuity, *Bull. Seism. Soc. Am.*, 61, 79-92.

Ryder, I., Parsons, B., Wright, T.J. & Funning, G.J., 2007. Post-seismic motion following the 1997 Manyi (Tibet) earthquake: InSAR observations and modelling, *Geophys. J. Int.*, 169, 10091027. doi:10.1111/j.1365-246X.2006.03312.x.

Savage, J. & Prescott, W., 1978. Asthenosphere readjustment and the earthquake cycle, *J. Geophys. Res.*, 83, 3369-3376.

Savage, J.C. & Svarc, J.L., 1997. Postseismic deformation associated with the 1992 Mw=7.3 Landers earthquake, southern California rupture, *J. Geophys. Res.*, 102, 7565-7577.

Savage, J.C., Svarc, J.L. & Yu, S.B., 2005. Postseismic relaxation and transient creep, *J. Geophys. Res. Solid Earth*, 110, 1-14. doi:10.1029/2005JB003687.1.

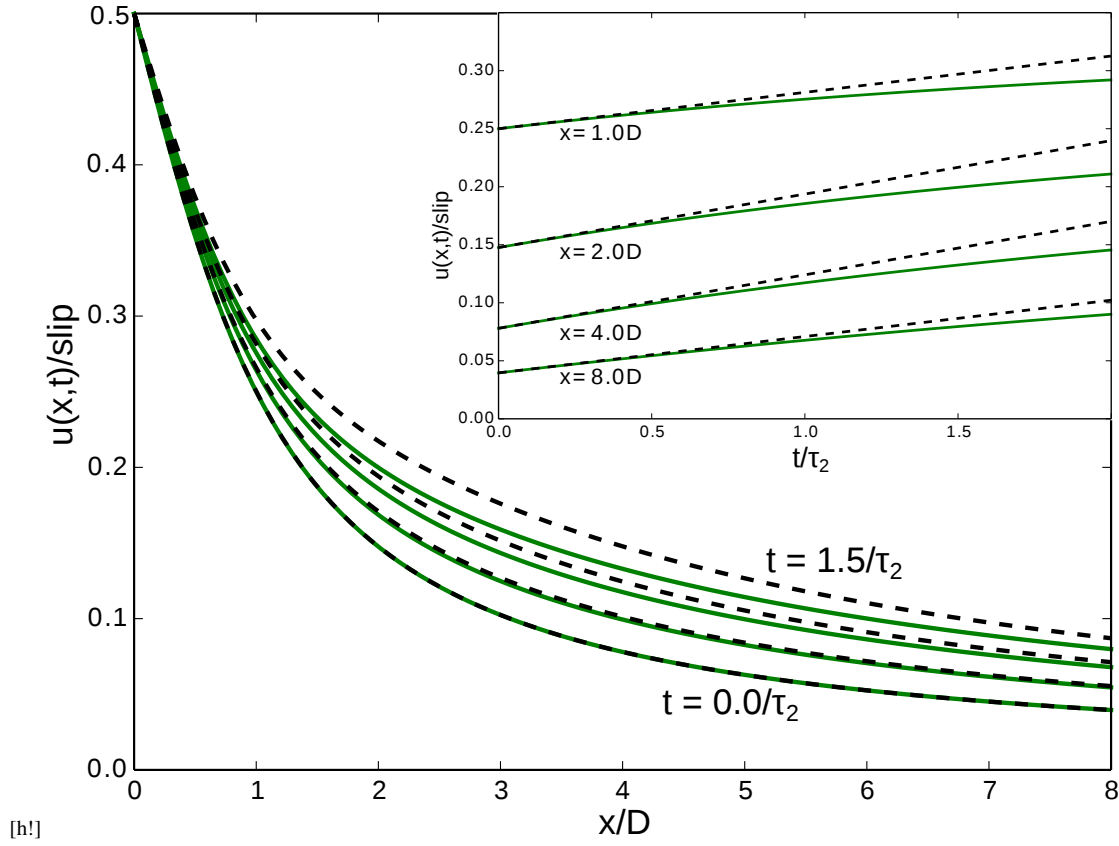Segall, P., 2010. Earthquake and volcano deformation, pp 185-186, Princeton University Press.

Figure A1. Surface displacements predicted by eq. (10) truncated after five terms (blue) and the approximation given by eq. (11) (dotted black). Displacements are shown at times 0, 5, 10, and 15 years following an earthquake
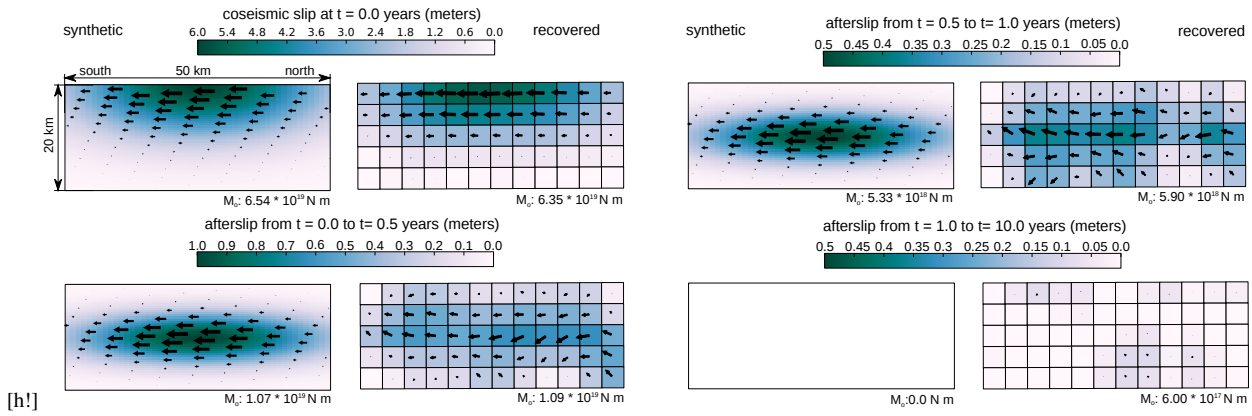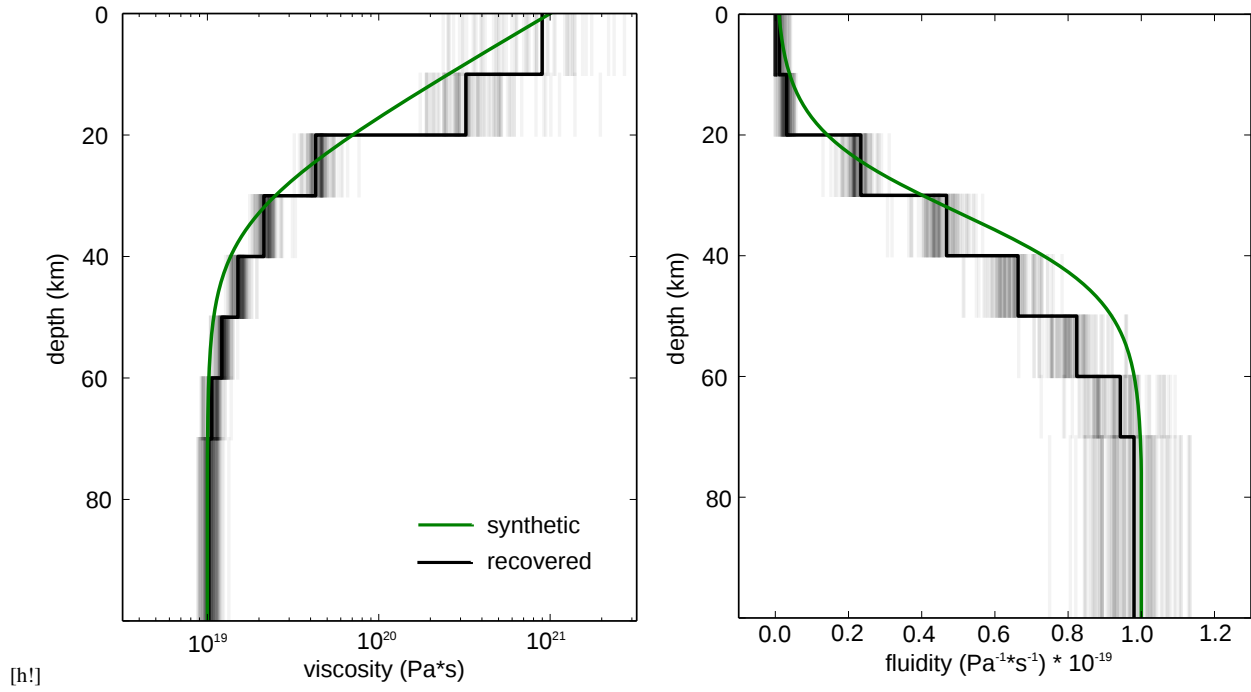

Figure A2. Left: slip distribution imposed in the synthetic model and slip recovered from the inversion. Colors indicate magnitude of slip and arrows indicate direction of slip (right is left lateral and up is thrust)

[h!]

Figure A3. Synthetic and recovered lithospheric viscosity strucutures. Blue line indicates viscosity structure imposed in the synthetic test. Black line indicates viscosity structure inferred from the synthetic surface displacement. Semi-transparent lines are recovered models found through bootstrapping and indicate the degree of uncertainty on the inferred viscosity structure. The left and right panels show the same information under different projections
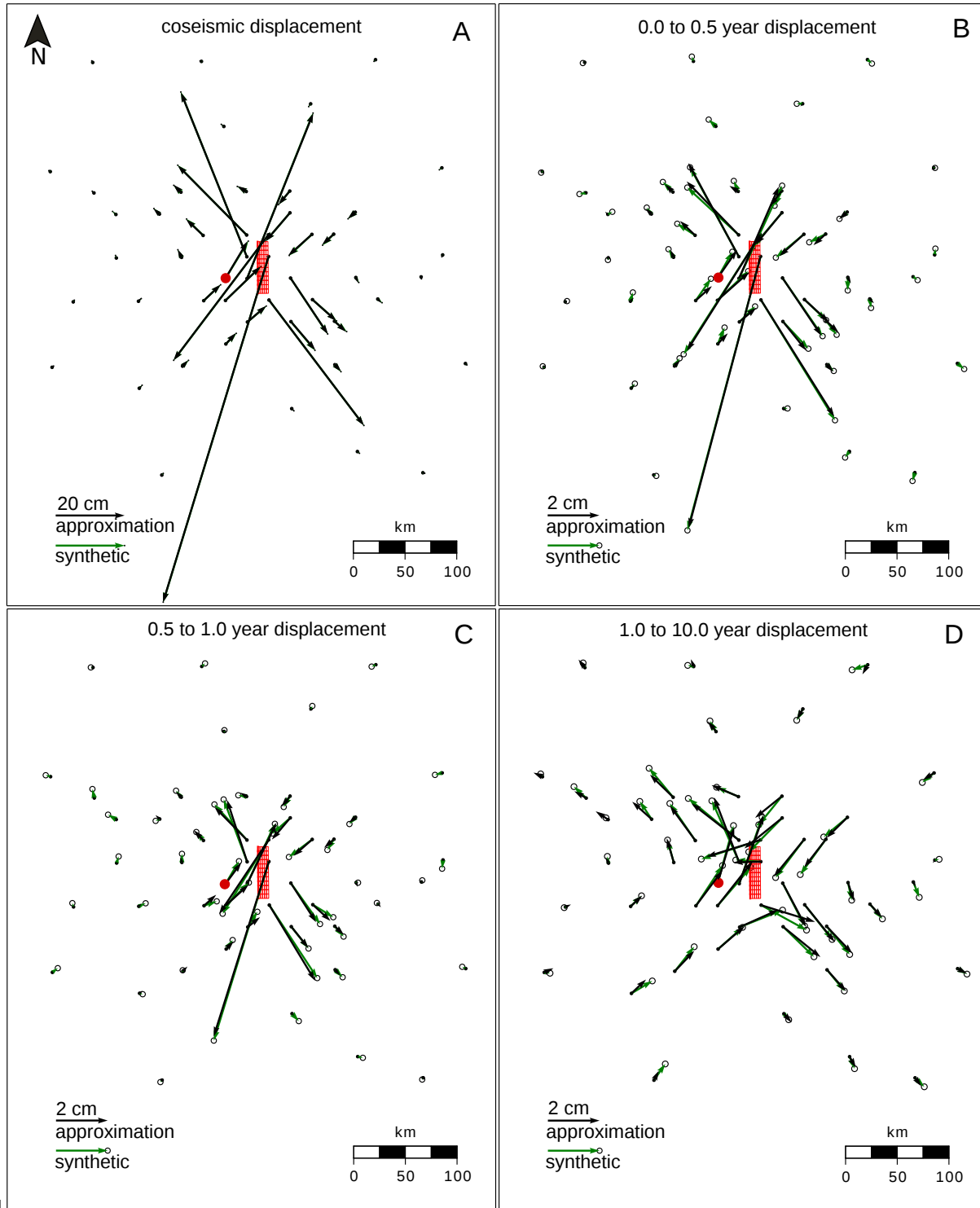
Figure A4. Synthetic surface displacements (blue) and best fitting surface displacements (black). Vertical displacements are used in the inversion but are not shown here. The top left panel shows coseismic displacements and the remaining panals show the displacements over the indicated time intervals. Red dot indicates the position whos time series is shown in figure 5. The red wireframe is the synthetic fault discretized into fault patches.
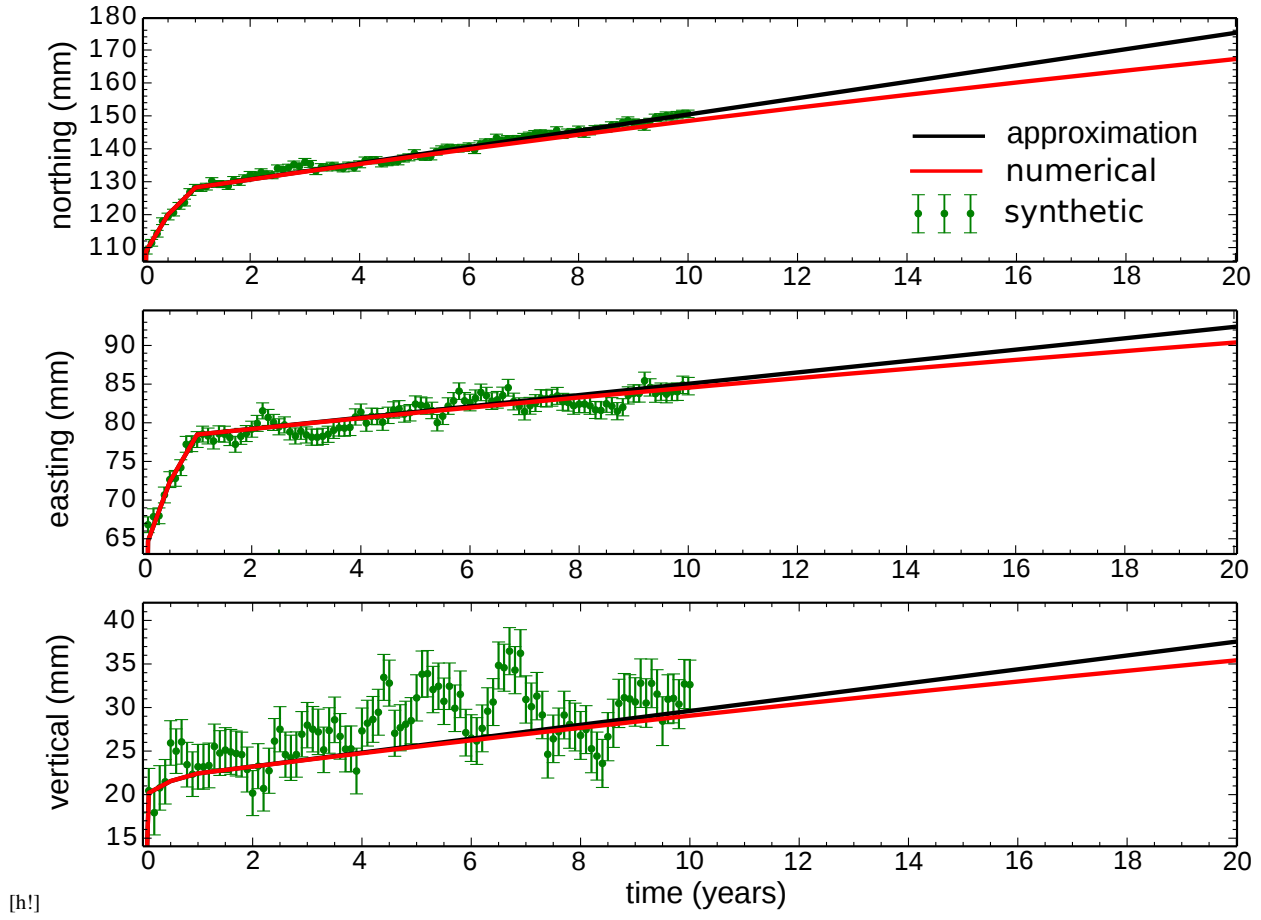
Figure A5. Displacement time series for the position shown in figure 4 (blue) and best fitting surface displacements using the approximation from eq. (18) (black). The red line indicates surface displacements computed using Pylith where the inferred slip distribution and viscosity structure are used as input. Values for displacement are with respect to the locations preseismic position.
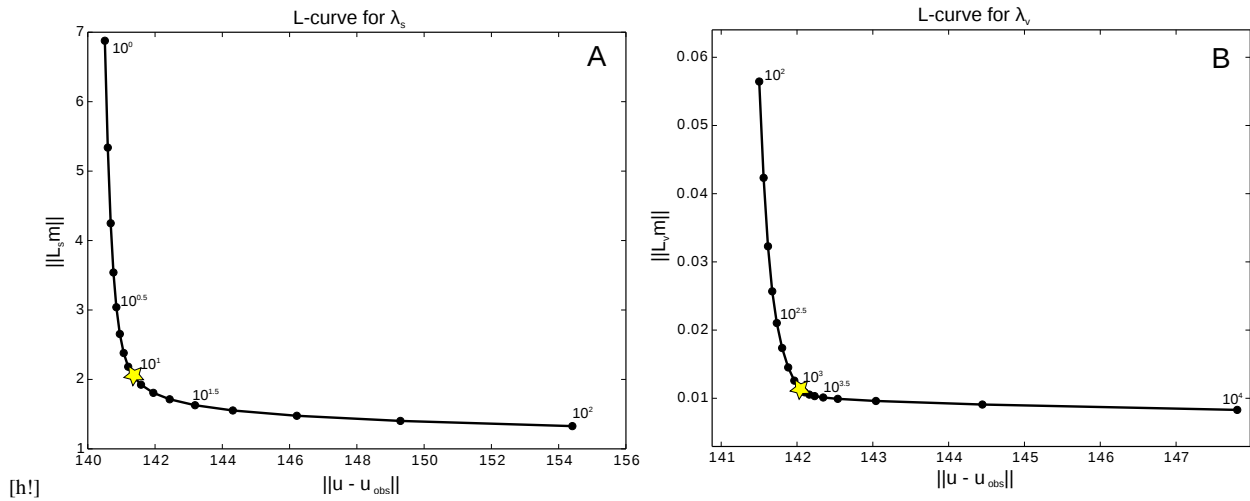

Figure A6. L-curves used to select the penalty parameters. Panel A shows the trade off between slip smoothness and data misfit while varying λ_s and keeping λ_v fixed at zero. Panel B shows tade off between smoothness of inferred viscosity and misfit while varying λ_v and keeping λ_s fixed at the value chosen from Panal A. Stars indicate our chosen penalty parameters.
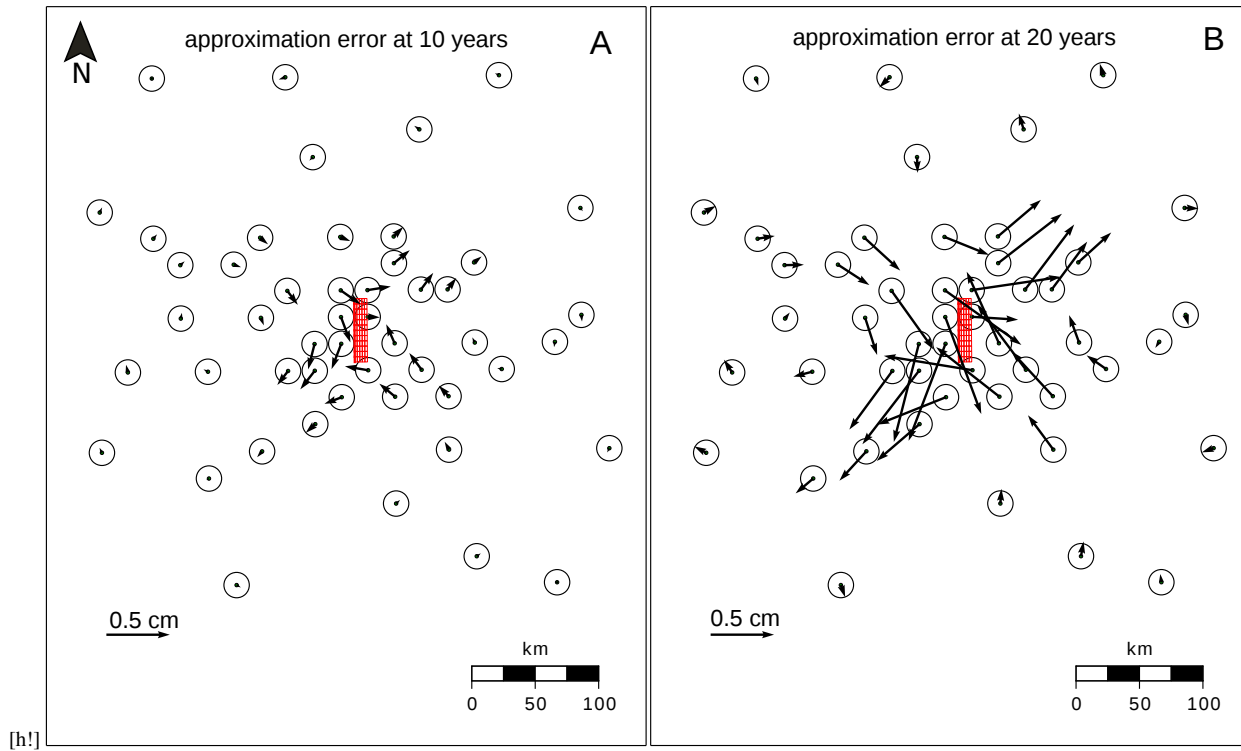
Figure A7. Difference between the surface displacement approximation and the numerically computed surface displacements. Top left panel shows the difference 10 years after the earthquake and the top right panel shows the difference at 20 years. The bottom panel shows the root mean square of the approximation error over time.